Plasticity in bulk metallic glasses investigated via the strain distribution

Jayanta Das,[1,*] Magnus Boström,[2] Norbert Mattern,[1] Åke Kvick,[3] Alain Reza Yavari,[4] Alan Lindsay Greer,[5] and Jürgen Eckert[1,†]

[1]*IFW Dresden, Institut für Komplexe Materialien, Helmholtzstraße 20, D-01069 Dresden, Germany*

[2]*Sandvik Materials Technology, SE-81181 Sandviken, Sweden*

[3]*European Synchrotron Radiation Facilities (ESRF), 38042 Grenoble, France*

[4]*LTPCM-CNRS UA29, Domaine Universitaire BP 75, Saint Martin d'Hères 38402, France*

[5]*Department of Materials Science and Metallurgy, University of Cambridge, Pembroke Street, Cambridge CB2 3QZ, United Kingdom*

(Received 21 August 2007; published 17 September 2007)

We measured the atomic-scale elastic strain in order to investigate the yielding of $Zr_{55}Cu_{20}Ni_{10}Al_{10}Ti_5$ and $Cu_{47.5}Zr_{47.5}Al_5$ bulk metallic glasses (BMGs) by x-ray synchrotron radiation at room temperature. High resolution strain scanning reveals a deviation from the linear stress-strain relationship at the onset of macroplastic flow. Similar to polycrystalline metals, a saturation of the elastic strain components has been revealed in the case of the "plastic" $Cu_{47.5}Zr_{47.5}Al_5$ BMG. The results show that the atomic-level elastic strains of the plastic $Cu_{47.5}Zr_{47.5}Al_5$ BMG are more homogeneous compared to the "brittle" $Zr_{55}Cu_{20}Ni_{10}Al_{10}Ti_5$ glass.

DOI: 10.1103/PhysRevB.76.092203 PACS number(s): 81.05.Kf, 62.20.Dc, 61.10.Eq

The response of high strength materials to an applied force is of interest for understanding the deformation mechanisms beyond the "reversible" elastic regime.[1] However, elastic strains play an important role on deformation-induced structural reorientation on the atomic/mesoscopic scale, which is responsible for creating macroscopic plastic strain.[2] The complex behavior of the loading path from the initial to the final state of stress and strain after permanent deformation tackles one of the crucial aspects of plasticity.[3] Typically, metals and alloys with fine grain size (<100 nm) (Ref. 4) possess high strength but show poor plastic deformability at room temperature. Experimental results suggest that the deformation process of these materials is strongly influenced by the strain interaction between structural defects such as dislocations,[5] chemistry at the grain boundaries,[6] stacking faults, and short-range order of the crystalline phases.[7] These brittle materials are notoriously susceptible to processing artifacts/preexisting flaws similar to ceramics, structurally disordered matter, or glasses even when tested under compression and show little plasticity, thus allowing for studies of their yield behavior.[8]

The theory of the plastic deformation processes in metallic glasses is related to shear transformation zones (STZs), where a cluster of atoms rearranges under an applied stress.[9] Shear bands initiate at certain preferred sites presumably due to stress concentrations.[10,11] Due to the absence of structural defects such as dislocations, the plastic strain in bulk metallic glasses (BMGs) is considered to be concentrated into these shear bands.[12] In the case of BMG composites, shear band propagation becomes limited because the stress state in the glassy matrix away from a second phase particle is insufficient to sustain its propagation.[13] As the strain increases, the crystalline particles are strain hardened and the stress continues to increase, and more and more initiation sites for shear bands are activated.[14,15] However, in some cases of compressive deformation of ceramics or glasses, where the defects in question are microcracks, the nominal flow stress may increase beyond the conventional sense of "work hardening," but this does not suppress shear localization.[16]

Strain scanning for determining the elastic strain tensor requires sophisticated and precise measurement techniques has been done by using the strain-gage rosettes on a microscopic scale for the two-dimensional state of stress (Mohr circle of strain).[2] Such studies can also be performed by using diffraction techniques on an atomic scale to correlate the mesoscopic and the microscopic strain.[17] Previous diffraction studies have been performed to reveal (i) the effect of hydrostatic stress state on the atomic-scale structural changes in glasses at high pressure,[18] (ii) the change of free volume during annealing,[19] (iii) the strain in the crystalline phase in glass-matrix composites,[20,21] and (iv) the strain tensor in monolithic BMG up to 200 MPa below the elastic limit.[22] It is well known that metallic glasses show plasticity during rolling,[23] but in recent years, several BMGs showing plasticity[24–28] in compression at room temperature in unconstrained geometry (height/diameter=2) have been found.[29] This allows for the characterization of BMGs during plastic yielding by diffraction methods.

In this Brief Report, we performed strain scanning by x-ray diffraction beyond the Hookean limit in order to investigate the plastic yielding phenomena of two different BMGs at higher resolution. The alloys are "plastic" $Cu_{47.5}Zr_{47.5}Al_5$ (Ref. 24) and macroscopically "brittle" $Zr_{55}Cu_{20}Ni_{10}Al_{10}Ti_5$ (Ref. 30) BMGs. The experiments have been performed using bulk parallelepiped specimens (2×2 mm^2) under unconstrained geometry at the European Synchrotron Radiation Facility (ID11) by *in situ* compressive loading in steps of 0.05 kN in a mechanical test rig carefully aligned to the beam using 80 keV x-rays ($\lambda=0.155$ Å, $\Delta\lambda<10^{-4}$).

Figures 1(a) and 1(b) show the diffraction patterns of the as-cast samples. Both diffraction patterns show diffuse scattering representing the amorphous nature of the specimens. The diffraction patterns are characterized with respect to the polar coordinates (r,θ) dividing 0°–360° into 36 segments using the FIT2D program. In order to analyze the strain tensor in the glassy specimens, a compressive load was applied and the two dimensional intensity distributions of the circular-

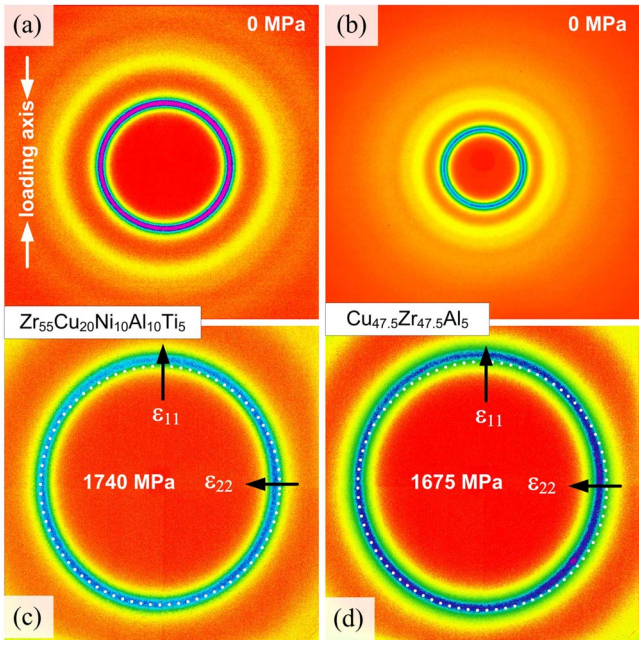

FIG. 1. (Color online) The diffraction patterns of $Zr_{55}Cu_{20}Ni_{10}Al_{10}Ti_5$ and $Cu_{47.5}Zr_{47.5}Al_5$ before [(a) and (b)] and after employing stress [(c) and (d)] near plastic yielding, showing a very clear change from circular to elliptical shape. A dotted circle is shown to reveal that the average interatomic spacing decreases along the loading axis (ϵ_{11}) and increases along the transverse direction (ϵ_{22}).

elliptical diffraction patterns were integrated azimuthally ±5° centered on the loading and the transverse axis.

The ring patterns for $Zr_{55}Cu_{20}Ni_{10}Al_{10}Ti_5$ and $Cu_{47.5}Zr_{47.5}Al_5$ at 1740 and 1675 MPa stresses are shown in Figs. 1(c) and 1(d), respectively. The patterns clearly show the elliptical nature of the ring after loading compared to a circular feature of the unloaded state [Figs. 1(a) and 1(b)]. This indicates a decrease of the atomic spacing of the nearest neighbors along the loading axis. A dotted circle is shown in Figs. 1(c) and 1(d) to reveal the change of the shape from the circular to the elliptical diffraction pattern. The data analysis has been performed by the q-space method in reciprocal space, as reported earlier.[22] In the case of each integrated intensity $I(q)$, the shift of the first halo is determined with respect to the unloaded condition.

Figure 2 shows the change of q with increasing load for the two different alloys. A very clear change of the q value of the first halo is visible from both the loading axis and the transverse axis. The change of the peak positions in q space has been measured[17] to be from average atomic spacing (d)=2.4112 Å (0 MPa) to d=2.3692 Å (1740 MPa), with an error of ±0.0002 Å in the case of $Zr_{55}Cu_{20}Ni_{10}Al_{10}Ti_5$ along the loading direction [Fig. 2(a)]. Similarly, in the case of $Cu_{47.5}Zr_{47.5}Al_5$, the peak shifts from d =2.3284 Å (0 MPa) to d=2.2937 Å (1506 MPa) with ±0.0002 Å [Fig. 2(b)]. In order to estimate the strain tensor quantitatively, the integrated data have been plotted by considering the average atomic spacing (d) versus the measured elastic scattering intensity $I(q)$ and a pseudo-Voigt function has been used in order to fit the first halo. The resulting d values at each different stress level were plotted, and the difference in d has been measured with respect to the unloaded condition as strain, as described earlier.[17,22] The axial (ϵ_{11}), transverse (ϵ_{22}), and shear (γ_{12}) components have been determined from the following equation:[2]

$$\epsilon_\theta = \epsilon_{11}\cos^2\theta + \gamma_{12}\cos\theta\sin\theta + \epsilon_{22}\sin^2\theta. \quad (1)$$

Figures 3(a) and 3(b) show the evolution of the different atomic-scale strain components (ϵ_{11}, ϵ_{22}, and γ_{12}) with applied stress for $Zr_{55}Cu_{20}Ni_{10}Al_{10}Ti_5$ and $Cu_{47.5}Zr_{47.5}Al_5$, respectively. In the case of $Zr_{55}Cu_{20}Ni_{10}Al_{10}Ti_5$, the strain components in the loading direction (ϵ_{11}) and transverse direction (ϵ_{22}) increase. However, the shear component γ_{12} values remain close to zero. However, the increment of ϵ_{11} and ϵ_{22} strains slightly deviates from linearity after 1400 MPa (a dotted line has been drawn to show the linearity of the elastic stress-strain relationship), and the sample broke at 1740 MPa with an axial strain ϵ_{11}=−0.0174 and a transverse strain ϵ_{22} of +0.00675. This strength value is similar to the macroscopic yielding (MY) of this alloy at 1727 MPa, as observed earlier.[30]

$Cu_{47.5}Zr_{47.5}Al_5$ shows [Fig. 3(b)] a very similar stress-strain relationship. However, the nonlinear stress-strain behavior starts at around 1200 MPa and, finally, the elastic strain saturates at a stress of 1506 MPa with an axial strain ϵ_{11}=−0.0150 and a transverse strain ϵ_{11}=+0.0056 without alteration of the shear component γ_{12}, which is close to 0. The test was stopped at 1700 MPa at a plastic strain of about 0.6%–0.7%. It is worth noting that the microscopic yield stress has been measured to be 1547 MPa for $Cu_{47.5}Zr_{47.5}Al_5$, as reported earlier.[24] Therefore, the stress required for macroscopic yielding under compression and the saturation of the elastic strain at the atomic scale are quite consistent for

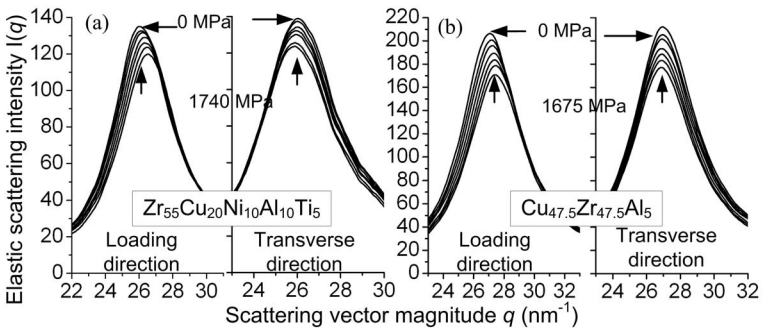

FIG. 2. Integrated elastic scattering intensity $I(q)$ versus scattering vector magnitude (q) at different employed stresses along loading and transverse axes for (a) $Zr_{55}Cu_{20}Ni_{10}Al_{10}Ti_5$ and (b) $Cu_{47.5}Zr_{47.5}Al_5$.

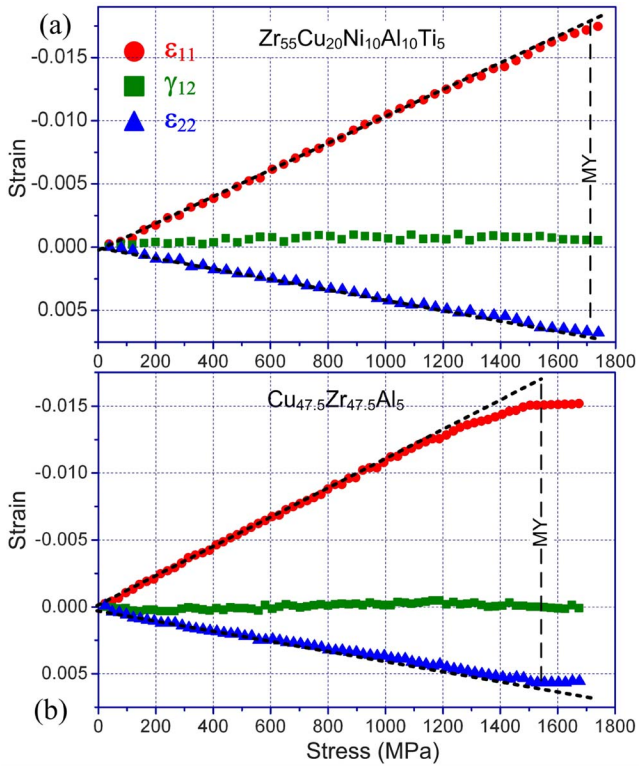

FIG. 3. (Color online) Evolution of elastic strain components of (a) $Zr_{55}Cu_{20}Ni_{10}Al_{10}Ti_5$ and (b) $Cu_{47.5}Zr_{47.5}Al_5$ during loading. The increment of ϵ_{11} and ϵ_{22} strains deviates from linearity on atomic scale before the onset of macroscopic yielding.

both the investigated alloys. We study such high resolution strain scanning by investigating the plastic yielding of BMGs and the observation of the nonlinear stress-strain behavior of a metallic glass in the elastic regime beyond the Hookean limit.[17,21,22]

The strain tensors for both the alloys have been calculated in the linear elastic region and diagonalized in order to estimate the elastic constants. Table I shows Young's modulus (E) and Poisson's ratio (ν) from the strain tensor and from ultrasonic sound velocity measured measurements: of 91.1 (GPa), 0.38 and 99.2 (GPa), 0.34 for $Zr_{55}Cu_{20}Ni_{10}Al_{10}Ti_5$ and $Cu_{47.5}Zr_{47.5}Al_5$, respectively. Poisson's ratio does not vary for the different measurements but Young's modulus varies between 6 and 8 GPa for the different alloys. Possibly, the stiffness of the first, second, and consecutive atomic shells are different, which can be detected from diffraction measurements, but the ultrasonic sound velocity technique averages the elastic constants of different shells, leading to the measurements of bulk properties of the material.

TABLE I. Elastic constants measured from the strain tensor (ST) and from ultrasonic sound velocity (USV) measurements: Young's modulus E (GPa) and Poisson's ratio ν.

Alloy composition	E_{ST}	ν_{ST}	E_{USV}	ν_{USV}
$Zr_{55}Cu_{20}Ni_{10}Al_{10}Ti_5$	91.1	0.38	85.5	0.378
$Cu_{47.5}Zr_{47.5}Al_5$	99.2	0.34	90.1	0.365

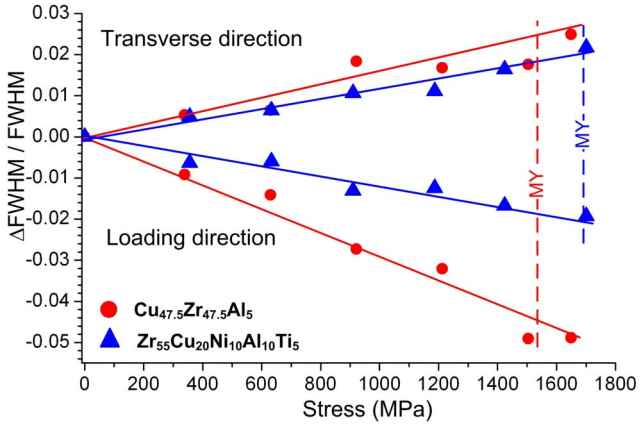

FIG. 4. (Color online) The change of width [full width at half maximum (FWHM)] with applied stress for the "plastic" $Cu_{47.5}Zr_{47.5}Al_5$ is higher than for the macroscopically "brittle" $Zr_{55}Cu_{20}Ni_{10}Al_{10}Ti_5$.

The nonlinear elastic behavior must be related to the deformation of topologically unstable short-range ordered clusters at the onset of the activation of STZs below plastic yielding.[31] The sluggish increase of the elastic strain and the deviation from linearity are more dominant in the case of plastic $Cu_{47.5}Zr_{47.5}Al_5$. This is indicative of structural rearrangements, which must also have occurred in $Zr_{55}Cu_{20}Ni_{10}Al_{10}Ti_5$. However, the total number of atoms/clusters may vary depending on the local atomic environments due to the alloy composition or the relaxed state of the glass. Such rearrangement of atoms by switching from one site to a neighboring one is not possible for all the atoms in the structure, but can occur preferentially in some regions where the local dilation is large enough to render the short-range order (SRO) to become topologically unstable with respect to the nucleation of STZs.

In order to understand the effect of atomic-level elastic strain distribution on yielding in BMGs, we have investigated the change of the width [full width at half maximum (FWHM)] of the first peak with applied stress. With increasing stress, the width of the peak decreases in the loading direction and increases in the transverse direction, as shown in Fig. 4. Interestingly, the change (ΔFWHM/FWHM) of the width under stress is significantly higher in plastic $Cu_{47.5}Zr_{47.5}Al_5$ than in brittle $Zr_{55}Cu_{20}Ni_{10}Al_{10}Ti_5$. The decrease of the width suggests that more SRO clusters take part in the elastic deformation and redistribute strain in the transverse direction. The more the stress increases, the higher the number of such entities becomes activated, and they realign themselves under the applied stress. Thus, the free volume can be more evenly redistributed and more averaging of the local hydrostatic stress can occur, reaching closer to the overall mean hydrostatic stress.[32] The more even stress distribution leads to a homogenous activity of the STZs, as can be observed from a large change in peak width (Fig. 4) and a larger deviation from the linear elastic behavior [Fig. 3(b)]. On the other hand, in the case of brittle glasses, the change of the peak width is rather sluggish due to the "jammed state" of STZs, which interact with locally quenched-in stress,

leading to a more inhomogeneous strain distribution and thus hindering the dynamics of the STZs in carrying plasticity.[9,33] However, it is worth mentioning that the same $Zr_{55}Cu_{20}Ni_{10}Al_{10}Ti_5$ BMG shows plasticity in the relaxed state after the annealing treatment and the yield stress drops from 1727 to 1647 MPa.[31] In addition, localized structural rearrangement can trigger the shear transformation to the surrounding neighboring atoms when the jammed state of the STZs transforms into an "unjammed" one.[9,33] Such autocatalytic inelastic shear processes can carry plasticity in a glassy structure at low temperature, as observed in the case of amorphous Si.[34] Therefore, a more even distribution of atomic-level elastic strain close to yielding of BMGs is the precursor of homogeneous activation of STZs, which can facilitate macroplastic flow.

In summary, we have observed a clear difference in the elastic deformation and atomic scale yielding behavior of different BMGs. The atomic-scale elastic strain components deviate from linearity when the stress approaches yielding. The elastic strain components saturate during the macroscopic flow of BMGs, similar to the case of crystalline materials. In the case of plastic BMGs, the distribution of elastic strain is rather homogeneous, which may trigger a homogeneous activity of shear transformations throughout the bulk volume of the specimen during yielding.

The authors are grateful for the financial support provided by the European Union within the framework of the Research Training Network on "ductile bulk metallic glass composites" (MRTN-CT-2003-504692).

*j.das@ifw-dresden.de
†Also at TU Dresden, Institut für Werkstoffwissenschaft, Helmholtzstraße 7, D-01069 Dresden, Germany.

[1] K. S. Kumar, H. Van Swygenhoven, and S. Suresh, Acta Mater. **51**, 5743 (2003).
[2] G. Dieter, *Mechanical Metallurgy*, 3rd ed. (McGraw-Hill, London, 1988).
[3] J. Schiøtz and K. W. Jacobsen, Science **301**, 1357 (2003).
[4] Y. M. Wang, M. W. Chen, F. H. Zhou, and E. Ma, Nature (London) **419**, 912 (2002).
[5] L. Lu, L. B. Wang, B. Z. Ding, and K. Lu, J. Mater. Res. **15**, 270 (2000).
[6] K. M. Youssef, R. O. Scattergood, K. Linga Murty, J. A. Horton, and C. C. Koch, Appl. Phys. Lett. **87**, 091904 (2005).
[7] J. Das, J. Eckert, and R. Theissmann, Appl. Phys. Lett. **89**, 261917 (2006).
[8] W. J. Kim, J. Wolfenstine, and O. D. Sherby, Acta Metall. Mater. **39**, 199 (1991).
[9] M. L. Falk and J. S. Langer, Phys. Rev. E **57**, 7192 (1998).
[10] A. S. Argon, J. Phys. Chem. Solids **43**, 945 (1982).
[11] F. Spaepen, Acta Metall. **25**, 407 (1977).
[12] J. J. Lewandowski and A. L. Greer, Nat. Mater. **5**, 15 (2006).
[13] E. Ma, Nat. Mater. **2**, 7 (2003).
[14] G. He, J. Eckert, W. Löser, and L. Schultz, Nat. Mater. **2**, 33 (2003).
[15] E. Pekarskaya, C. P. Kim, and W. L. Johnson, J. Mater. Res. **16**, 2513 (2001).
[16] B. R. Lawn, N. P. Padture, H. D. Cai, and F. Guiberteau, Science **263**, 1114 (1994).
[17] T. C. Hufnagel, R. T. Ott, and J. Almer, Phys. Rev. B **73**, 064204 (2006).
[18] H. W. Sheng, H. Z. Liu, Y. Q. Cheng, J. Wen, P. L. Lee, W. K. Luo, S. D. Shastri, and E. Ma, Nat. Mater. **6**, 192 (2007).
[19] A. R. Yavari, A. Le Moulec, A. Inoue, N. Nishiyama, N. Lupu, E. Matsubara, W. J. Botta, G. Vaughan, M. Di Michiel, and Å. Kvick, Acta Mater. **53**, 1611 (2005).
[20] R. T. Ott, F. Sansoz, J. F. Molinari, J. Almer, K. T. Ramesh, and T. C. Hufnagel, Acta Mater. **53**, 1883 (2005).
[21] D. K. Balch, E. Ustundag, and D. C. Dunand, Metall. Mater. Trans. A **34A**, 1787 (2003).
[22] H. F. Poulsen, J. A. Wert, J. Neuefeind, V. Honkimaki, and M. Daymond, Nat. Mater. **4**, 33 (2005).
[23] Y. Yokoyama, K. Inoue, and K. Fukaura, Mater. Trans., JIM **43**, 3199 (2002).
[24] J. Das, M. B. Tang, K. B. Kim, R. Theissmann, F. Baier, W. H. Wang, and J. Eckert, Phys. Rev. Lett. **94**, 205501 (2005).
[25] Y. Zhang, W. H. Wang, and A. L. Greer, Nat. Mater. **5**, 857 (2006).
[26] J. Schroers and W. L. Johnson, Phys. Rev. Lett. **93**, 255506 (2004).
[27] X. J. Gu, A. G. McDermott, S. J. Poon, and G. J. Shiflet, Appl. Phys. Lett. **88**, 211905 (2006).
[28] Y. H. Liu, G. Wang, R. J. Wang, D. Q. Zhao, M. X. Pan, and W. H. Wang, Science **315**, 1385 (2007).
[29] Z. F. Zhang, H. Zhang, X. F. Pan, J. Das, and J. Eckert, Philos. Mag. Lett. **85**, 513 (2005).
[30] K. Hajlaoui, A. R. Yavari, A. Le Moulec, W. J. Botta, G. Vaughan, J. Das, A. L. Greer, and Å. Kvick, J. Non-Cryst. Solids **353**, 327 (2007).
[31] A. V. Sergueeva, N. A. Mara, J. D. Kuntz, E. J. Lavernia, and A. K. Mukherjee, Philos. Mag. **85**, 2671 (2005).
[32] D. Srolovitz, V. Vitek, and T. Egami, Acta Metall. **31**, 335 (1983).
[33] L. Pechenik, Phys. Rev. E **72**, 021507 (2005).
[34] Michael J. Demkowicz and Ali S. Argon, Phys. Rev. B **72**, 245205 (2005).